

**Spin-orbit sensitive hard x-ray probe of the occupied and unoccupied  $5d$  density of states**Nikolay Smolentsev,<sup>1,2</sup> Marcin Sikora,<sup>3</sup> Alexander V. Soldatov,<sup>2</sup> Kristina O. Kvashnina,<sup>1</sup> and Pieter Glatzel<sup>1,\*</sup><sup>1</sup>European Synchrotron Radiation Facility, rue Jules Horowitz 6, 38043 Grenoble, France<sup>2</sup>Research Center for Nanoscale Structure of Matter, Southern Federal University, str. Sorge 5, 344090 Rostov-na-Donu, Russia<sup>3</sup>AGH University of Science and Technology, Al. Mickiewicza 30, 30-059 Krakow, Poland

(Received 20 July 2011; revised manuscript received 8 November 2011; published 5 December 2011)

We discuss a truly bulk sensitive,  $j$ -selective probe of the valence and conduction bands of the  $5d$  transition metal systems. The electronic structure of Re and W oxides, with formal occupation of  $d$ -states ranging from  $5d^0$  to  $5d^3$ , was investigated by means of resonant x-ray emission spectroscopy (RXES) across the  $L_3$  and  $L_2$  edges of Re ( $\sim 10.5$  and  $\sim 12$  keV, respectively) and W ( $\sim 10$  and  $\sim 11.5$  keV, respectively). We present a systematic theoretical analysis of the RXES spectra within a density functional theory band structure approach. Excellent agreement between experiment and theory is achieved, demonstrating that the theory accounts for the most relevant interactions within the experimental energy bandwidth ( $\sim 2$ – $3$  eV). Differences between the  $L_3$  and the  $L_2$  edges can be reproduced by considering spin-orbit interaction. The possible applications and limitations of our approach are discussed.

DOI: [10.1103/PhysRevB.84.235113](https://doi.org/10.1103/PhysRevB.84.235113)

PACS number(s): 71.20.-b, 78.70.Dm, 78.70.En, 71.70.Ej

**I. INTRODUCTION**

The role of spin-orbit interactions (SOIs) in condensed matter systems is drawing attention,<sup>1–6</sup> and there are intense research efforts to elucidate the physics of novel materials with  $5d$  electrons. SOI is especially important for  $5d$  elements because it increases proportionally with  $Z^4$ . It is crucial for understanding phenomena such as Mott transitions<sup>1–5</sup> and colossal magnetoresistance<sup>7</sup> in  $5d$  element-based compounds. It is often desirable to study valence and conduction bands of these systems using an element-selective and bulk sensitive probe that allows studies in extreme conditions (*e.g.*, high pressure and high temperature). For this, it is necessary to photoexcite the system at the  $2p_{3/2}$  or  $2p_{1/2}$  core level ( $L_3$  or  $L_2$  absorption edge) that lies above 10 keV and thus is in the hard x-ray range.

The x-ray absorption near edge structure (XANES) and x-ray emission spectroscopy (XES) are sensitive to the unoccupied and occupied partial density of states (DOS) near the Fermi level, respectively. Both techniques are combined in resonant x-ray emission spectroscopy (RXES) (or direct resonant inelastic x-ray scattering, or RIXS) that is a photon-in-photon-out process. In RXES, both the incoming and the outgoing x-rays are monochromatized with an energy bandwidth on the order of the core hole lifetime broadening.<sup>8,9</sup> In the present study, we apply core-to-valence RXES, where the emitted photon has an energy that corresponds to transitions from the valence band to a core state that was created by the incoming photon. XANES spectra are broadened by the lifetime of the core hole in the excited state. In  $L$ -edges of  $5d$  transition metals, the full width at half maximum (FWHM) of the core level is larger than 5 eV and important information in the electronic structure is often concealed. The excited final states in core-to-valence RXES do not exhibit a core hole and thus have a long lifetime. The main contribution to the spectral broadening here is the experimental resolution, providing the possibility to greatly enhance the spectral features.<sup>10,11</sup> Taking into account dipole selection rules, transitions to the  $d_{3/2}$  band are allowed at the  $L_2$  edge, whereas transitions to the entire  $d$ -band are observed at the  $L_3$  edge. This allows study

of the electronic structure with an element- and  $j$ -selective technique.

We present an experimental and theoretical study of the W and Re  $d$ -DOSs in  $WO_3$ ,  $ReO_3$ ,  $WO_2$ , and  $ReO_2$  with formal  $5d$  occupation ranging from  $5d^0$  to  $5d^3$  by means of the RXES at  $L_3$  and  $L_2$  absorption edges of W (10 206 and 11 548 eV, respectively) and Re (10 536 and 11 967 eV, respectively). We show that a simplified theoretical approach based on SOI band structure density functional theory (DFT) calculations successfully models the experimental data within the experimental resolution.

**II. EXPERIMENTAL DETAILS**

The measurements were performed at beamline ID26 of the European Synchrotron Radiation Facility (ESRF). Higher harmonics were suppressed by a flat Pd-coated and two bent Cr-coated mirrors operating in total reflection. The incident energy was selected by means of a pair of cryogenically cooled Si crystals in (311) reflection with an energy bandwidth of  $\sim 0.5$  eV at 10.5 keV. The incident flux on the sample was estimated to be  $5 \times 10^{12}$  photons/s. The beam size, measured as the FWHM of the integrated intensity profile, was 0.2 mm vertical by 1.0 mm horizontal. The resonantly emitted (scattered) x-rays were analyzed using the Bragg reflection of spherically bent Si single-crystal wafers. The  $\langle 555 \rangle$  reflection was used at the  $L_3$  edges of W (10 206 eV) and Re (10 536 eV). The  $\langle 933 \rangle$  reflection was used at the  $L_2$  edges of W (11 548 eV) and Re (11 967 eV). Sample, analyzer crystals and an avalanche photodiode were arranged in a vertical Rowland geometry ( $R = 1$  m) at a  $90 \pm 3^\circ$  horizontal scattering angle to minimize the intensity of Thomson (elastic) scattering. The combined instrumental energy bandwidth, measured as the FWHM of the elastic peak, was estimated to be 2.0 (2.8) and 2.5 (3.2) eV in the W  $L_2$  ( $L_3$ ) and Re  $L_3$  ( $L_2$ ) spectral ranges, respectively. All samples studied were fine powders of the highest commercially available purity (more than 99.7%) purchased from Sigma-Aldrich and prepared as pressed into thick pellets.

### III. THEORETICAL APPROACH

The resonant scattering of a photon in matter is described by the Kramers-Heisenberg equation at resonance<sup>12,13</sup>

$$\frac{d\sigma_{\text{resonant}}(\omega_1, \omega_2)}{d\Omega} = \frac{r_e^2 \omega_2}{m_e^2 \omega_1} \sum_f \left| \sum_n \frac{\langle f | T_2 | n \rangle \langle n | T_1 | g \rangle}{E_n - E_g - \omega_1 - i \frac{\Gamma_n}{2}} \right|^2 * \frac{\frac{\Gamma_f}{2\pi}}{(E_g - E_f + \omega_1 - \omega_2)^2 + \frac{\Gamma_f^2}{4}}, \quad (1)$$

where  $d\sigma/d\Omega$  is the differential cross section;  $\omega_1$  and  $\omega_2$  are the incident and emitted photon energies, respectively;  $|f\rangle$  is the final state,  $|n\rangle$  is the intermediate state, and  $|g\rangle$  is an initial state with energies  $E_f$ ,  $E_n$ , and  $E_g$ , respectively; and  $\Gamma_n$  and  $\Gamma_f$  are the lifetimes (in FWHM) of the intermediate states and the final states, respectively. The dipole operator for the incoming and outgoing beam is given by  $T_1$  and  $T_2$ , respectively. The classical radius and mass of the electron are given by  $r_0$  and  $m_0$ , respectively.

The main challenge of a theoretical treatment is the description of the multielectronic states, in particular the excited states  $|n\rangle$  and  $|f\rangle$ . The computational effort can be greatly reduced by applying some approximations that simplify the equation. First, we neglect interference effects between absorption and emission process and write

$$\frac{d\sigma_{\text{resonant}}}{d\Omega} = \frac{r_e^2 \omega_2}{m_e^2 \omega_1} \sum_f \sum_n \frac{\langle f | T_2 | n \rangle^2 \langle n | T_1 | g \rangle^2}{(E_g - E_n + \omega_1)^2 + \frac{\Gamma_n^2}{4}} * \frac{\frac{\Gamma_f}{2\pi}}{(E_g - E_f + \omega_1 - \omega_2)^2 + \frac{\Gamma_f^2}{4}}. \quad (2)$$

Then we neglect many-body effects for the calculation of absorption ( $\langle n | T_1 | g \rangle$ ) and emission ( $\langle f | T_2 | n \rangle$ ) transition matrix elements:

$$\langle n | T_1 | g \rangle^2 \propto \langle \phi_n | T_1 | \phi_g \rangle^2 \quad (3)$$

$$\langle f | T_2 | n \rangle^2 \propto \langle \phi_f | T_2 | \phi_n \rangle^2 \quad (4)$$

where  $|\phi_f\rangle$ ,  $|\phi_n\rangle$ , and  $|\phi_g\rangle$  are final, intermediate, and initial eigenstates of the effective one-electron Hamiltonian, respectively. The transition matrix elements can be calculated using the partial, *i.e.*, according to the dipole selection rules, DOS  $\rho(\varepsilon)$  multiplied with the radial transition probability  $M(\varepsilon)$ <sup>14</sup> ( $M(\varepsilon)$  is referred to as the squared matrix element<sup>8</sup>):

$$\langle \phi_n | T_1 | \phi_g \rangle^2 = M(\varepsilon_u) \rho'(\varepsilon_u) \approx \rho'(\varepsilon_u) \quad (5)$$

for the unoccupied DOS  $\rho'(\varepsilon_u)$  with energy  $\varepsilon_u$  and

$$\langle \phi_f | T_2 | \phi_n \rangle^2 = M(\varepsilon_o) \rho(\varepsilon_o) \approx \rho(\varepsilon_o) \quad (6)$$

for the occupied DOS  $\rho(\varepsilon_o)$  with energy  $\varepsilon_o$ .

The angular momentum projected (partial) DOS is used. The dipole selection rule is  $\Delta l = \pm 1$ , but we neglect transitions from  $p(l=1)$  to  $s(l=0)$  because the  $\Delta l = -1$  calculated radial transition probability is  $\sim 10$  times smaller than for  $\Delta l = +1$  in the present case. Furthermore, the  $s$ -DOS around the Fermi level is  $\sim 10$  times smaller than the  $d$ -DOS. We assume  $M(\varepsilon)$  to be constant but evaluate this simplification (see Sec. V.D).  $M(\varepsilon)$  is identical for transitions to occupied and unoccupied

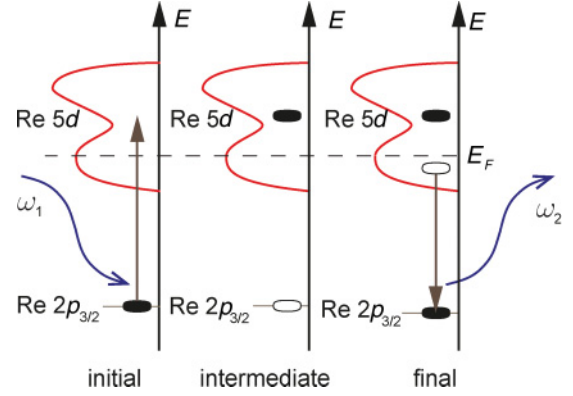


FIG. 1. (Color online) Simplified energy diagram for the RXES process at the Re  $L_3$  edge.

states in the case of core-to-valence RXES. We approximate  $\omega_1/\omega_2 \approx 1$  in Eq. (2) because of the short energy range in core-to-valence RXES. Then we replace the sum in Eq. (2) with an integral:

$$\frac{d\sigma_{\text{resonant}}}{d\Omega} \propto \int_{\varepsilon_o} d\varepsilon_o \int_{\varepsilon_u} d\varepsilon_u \frac{\rho(\varepsilon_o) \rho'(\varepsilon_u)}{(\omega_1 - \varepsilon_u)^2 + \frac{\Gamma_n^2}{4}} * \frac{\frac{\Gamma_f}{2\pi}}{(\varepsilon_o - \varepsilon_u + \omega_1 - \omega_2)^2 + \frac{\Gamma_f^2}{4}}. \quad (7)$$

Assuming very long-lived final states, we replace the second Lorentzian with a Dirac  $\delta$ -function:

$$\frac{d\sigma_{\text{resonant}}}{d\Omega} \propto \int_{\varepsilon_o} d\varepsilon_o \int_{\varepsilon_u} d\varepsilon_u \frac{\rho(\varepsilon_o) \rho'(\varepsilon_u)}{(\omega_1 - \varepsilon_u)^2 + \frac{\Gamma_n^2}{4}} * \delta(\varepsilon_o - \varepsilon_u + \omega_1 - \omega_2). \quad (8)$$

After integration, we obtain

$$\frac{d\sigma_{\text{resonant}}(\omega_1, \omega_2)}{d\Omega} \propto \int_{\varepsilon} d\varepsilon \frac{\rho(\varepsilon) \rho'(\varepsilon + \omega_1 - \omega_2)}{(\varepsilon - \omega_2)^2 + \frac{\Gamma_n^2}{4}}. \quad (9)$$

This formula was first reported in Ref. 15. The simplified RXES process is schematically shown in Fig. 1. All RXES maps in this paper were calculated using this formula. Only transitions to  $d_{3/2}$  orbitals are allowed at the  $L_2$  edge, whereas transitions to both  $d_{3/2}$  and  $d_{5/2}$  are allowed at the  $L_3$  edge. An elastic peak due to Thomson scattering was added to the RXES planes to facilitate comparison with experiment. The following values were used for the lifetime broadening of the  $2p_{3/2}$  and  $2p_{1/2}$  core holes: 4.98 and 5.33 eV for W, respectively, and 5.04 and 5.48 eV for Re, respectively.<sup>16</sup> All calculated RXES maps were convoluted with additional Gaussian broadening of 0.8 eV for emitted energy and 0.3 eV for incident energy.

### IV. CALCULATIONAL DETAILS

Crystallographic data were taken from the Inorganic Crystal Structure Database (ICSD).<sup>17</sup> We used the following space groups:  $Pm-3m$  for  $\text{ReO}_3$ ,  $Pbcn$  for  $\text{ReO}_2$ ,  $P21/n$  for  $\text{WO}_3$ , and  $P21/c$  for  $\text{WO}_2$ . We used the full-potential, self-consistent Wien2k code<sup>14</sup> to calculate the electronic structure of Re and W oxides (in particular, the angular momentum projected DOS) within the framework of DFT. For the exchange-correlation

potential, we used the generalized gradient approximation form derived by Perdew *et al.*<sup>18</sup> The basis functions for the valence orbitals were expanded simultaneously as spherical harmonics (inside nonoverlapping atomic spheres centered at the atomic sites) and as plane waves in the interstitial region. The plane waves were expanded up to a cutoff parameter,  $k_{\max}$ , fulfilling the relation  $R_A k_{\max} = 7$ , where  $R_A$  is the radius of the smallest atomic sphere. We used an atomic radius of 0.93 Å for Re and W atoms and 0.81 Å for oxygen atoms. The energy separation value between valence and core orbitals was set to 91 eV for Re oxides and 82 eV for W oxides. The self-consistent iteration process was repeated until an energy convergence of  $1.3 \times 10^{-3}$  eV was reached. The number of  $k$ -points in the Brillion zone was set to 1000 for ReO<sub>2</sub>, WO<sub>2</sub>, and ReO<sub>3</sub> and 300  $k$ -points for WO<sub>3</sub> as a compromise between precision and computational time. We used second variational treatment of SOL.<sup>19</sup> In this approach, wave functions were first calculated in the scalar relativistic approximation for spin up and spin down. After that, these functions were used as basis functions. Then, a term describing SOI was added and the new eigenvalue problem for calculation of the new wave functions in both spin directions simultaneously was solved. The calculated DOS was projected on the  $d_{3/2}$  and  $d_{5/2}$  relativistic states to analyze the differences between the L<sub>2</sub> and the L<sub>3</sub> edge RXES maps. The  $d$ -DOS (total  $d$ -DOS for the L<sub>3</sub> edge, but only  $d_{3/2}$  for the L<sub>2</sub> edge) inside the  $5d$  transition metal atomic sphere was inserted into Eq. (9) to calculate the theoretical RXES planes. Theoretical values of the incident energies were shifted to the experimental ones. All results presented in this paper were calculated using Wien2k.

Calculations using full-multiple scattering theory within a muffin-tin potential approximation (FEFF9 code<sup>20</sup>) were also performed for comparison. Hedin-Lundquist exchange correlation with full core-hole screening was used. A cluster of radius 8 Å was used for the full multiple scattering calculations,

and two coordination shells were used for the calculation of the self-consistent potential. All other parameters were set to default values. The obtained  $d$ -DOS was used for the calculation of the RXES maps. X-ray emission spectra both in the dipole and in the quadrupole approximation were calculated to estimate the strength of quadrupole transitions.

## V. RESULTS AND DISCUSSION

### A. Assignment of general RXES features

The experimental RXES planes around the L<sub>3</sub> edge for ReO<sub>3</sub> and WO<sub>3</sub> are shown in Fig. 2(b) and 2(c). The energy difference between incident and emitted x-ray energy is the energy transfer or final state energy. The main features present in all spectra are an elastic peak, which extends as a horizontal streak through the plane; a main peak (from 0 to 15 eV energy transfer); a small feature at 25 eV energy transfer; and an intense peak at 35 eV for W oxides and 45 eV for Re oxides. The elastic peak allows determination of the zero energy transfer and provides an absolute energy calibration. This greatly facilitates comparison among experimental data, because experimental errors such as energy drifts are largely eliminated.

The Re (W)  $4f$  orbitals are split into  $4f_{5/2}$  and  $4f_{7/2}$  with binding energies of 43 (33.6) and 40.5 (31.4) eV, respectively.<sup>16</sup> The calculations do not show any Re or W  $d$ -DOS in the energy range of the  $4f$  orbitals; we therefore assign the spectral features  $\sim 45$  and 35 eV for Re and W, respectively, to quadrupole transitions from the  $4f$  orbitals. The reason for the strong spectral intensity (comparable to the  $5d$ -to- $2p$  dipole transitions) is that the  $2p$  and  $4f$  wavefunctions have significant overlap and both are strongly localized. The  $4f$  electron density of Re and W is distributed mainly within 0.4 Å around the atomic nucleus. Re and W  $2p$ -states are also situated within this sphere. The quadrupole emission peak

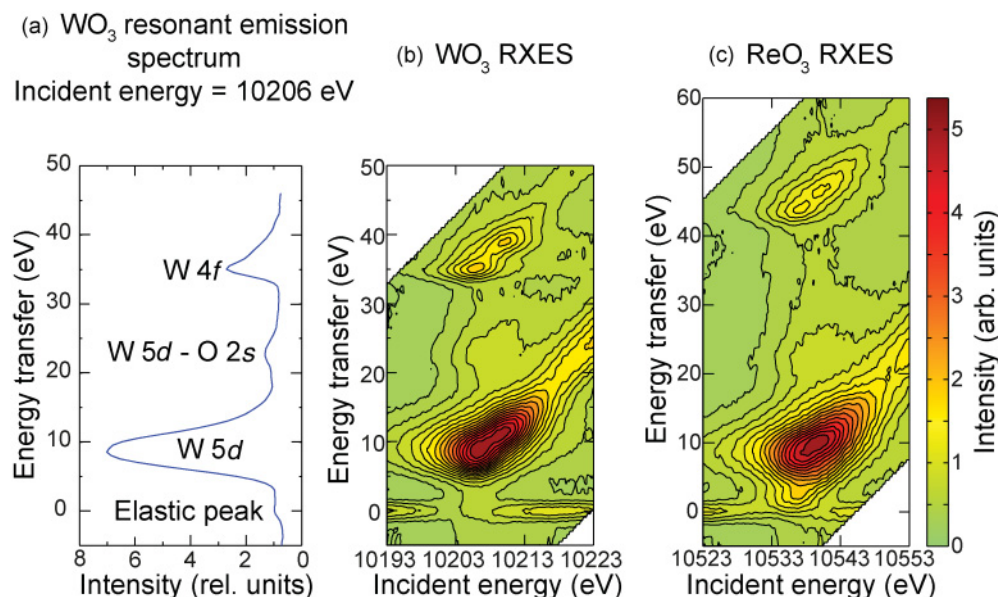


FIG. 2. (Color online) (a) Resonant emission spectrum of WO<sub>3</sub> recorded at 10206 eV incident energy (corresponding to a vertical cut through the RXES plane). Core-to-valence RXES planes for the L<sub>3</sub> edge for (b) WO<sub>3</sub> and (c) ReO<sub>3</sub>. The energy transfer is the difference between incident and emitted photon energies. The same color scale (0 = light to 5 = dark) is used for all subsequent figures.

is well reproduced in the calculation, taking into account quadrupole transitions (using the FEFF9 code, not shown). These quadrupole transitions were reported in conventional XES for metallic W and Re.<sup>21,22</sup>

A metal  $d$ -band appears in the range 0–15 eV for energy transfer of the RXES plane.  $\text{WO}_3$ , with the formal W valence state VI, has a formally empty  $5d$  band. An electron resonantly excited into the  $5d$  band that decays back into the  $2p$  shell only gives rise to an elastic scattered line in absence of any multielectron excitations.<sup>23,24</sup> Thus, inelastic features up to 15 eV for the final state energy should be absent for a fully empty  $5d$  DOS if one-electron transitions only are considered. The experimental RXES plane for  $\text{WO}_3$  shows, however, strong spectral features of  $\sim 10$  eV energy transfer. Calculations show indeed significant metal  $d$ -DOS below Fermi level (*cf.* Fig. 7).

Figure 2(a) shows an emission spectrum recorded at an incident energy of 10 206 eV with an assignment of the spectral features following our analysis. We assign the feature at  $\sim 20$  eV energy transfer to oxygen  $s$ -states that mix with the metal  $d$ -states (*cf.* Fig. 7). This assignment is in agreement with what has been observed for the valence-to-core transitions in  $3d$  transition metal compounds and has been referred to as “crossover” or  $K\beta'$  transition.<sup>9,25</sup>

The experimental and calculated RXES maps for  $\text{ReO}_3$ ,  $\text{WO}_3$ ,  $\text{ReO}_2$ , and  $\text{WO}_2$  at the  $L_2$  and  $L_3$  edges are presented in Fig. 3. We show RXES maps up to a 30 eV energy transfer for investigation of the partially filled  $5d$  band only. First, we focus on the main spectral features that are identical for both edges.  $\text{ReO}_3$  and  $\text{WO}_3$  exhibit similar RXES planes apart from a small low-energy transfer peak at 2 eV for  $\text{ReO}_3$ . Both compounds have octahedral coordination around the metal atom, which is slightly distorted for  $\text{WO}_3$  (*cf.* Fig. 4). The dominant feature in the RXES plane extends diagonally through the RXES plane (at constant emission energies).  $\text{WO}_3$  shows semiconducting behavior; *i.e.* it exhibits a band gap of  $\sim 3$  eV.<sup>26</sup> Consequently, the main RXES feature and the elastic peak are clearly separated by  $\sim 3$  eV. The three other oxides are metallic, and no gap is observed between the elastic peak and the resonant features; *i.e.* the elastic peak merges with the RXES features. The observed gap between the elastic peak and the resonant features directly shows the gap in the  $d$ -DOS. The elastic peak merges with the resonant features for systems without a band gap in the dipole-allowed DOS (*i.e.* for metallic systems). For  $\text{ReO}_2$  and  $\text{WO}_2$ , the strongest feature exhibits two prominent peaks at 5 and 10 eV energy transfer with slightly different intensities. The RXES planes of  $\text{WO}_2$  show a third peak at 3 eV energy transfer, which is not well resolved at the  $L_3$  edge and becomes much larger at the  $L_2$  edge. The continuum excitations extend as diagonal bands toward the highest incident energies in experiment and theory. These fluorescence features correspond to excitation of the photoelectron to the continuum  $d$ -band and subsequent emission from the  $5d$  valence band.

Figure 4 shows crystal structures of all studied oxides.  $\text{ReO}_3$  and  $\text{WO}_3$  are perovskite-like materials. The structure of  $\text{ReO}_3$  is similar to the perovskite structure ( $ABO_3$ ), without the large  $A$  cation at the center of the unit cell. Each Re atom is surrounded by six oxygen atoms, forming a  $\text{ReO}_6$  octahedron. These octahedrons are situated along the  $c$ -axis.  $\text{WO}_3$  has a similar structure, but the oxygen octahedrons are

slightly displaced off the  $c$ -axis.  $\text{WO}_2$  has a distorted rutile structure.  $\text{ReO}_2$  has an orthorhombic structure. The Re atom coordination in  $\text{ReO}_2$  is similar to the coordination of W in  $\text{WO}_2$ . The RXES maps for  $\text{WO}_3$  and  $\text{ReO}_3$  have similar features and are significantly different from those for  $\text{WO}_2$  and  $\text{ReO}_2$ . Therefore, the shape of the RXES map up to an energy transfer of  $\sim 15$  eV reflects the difference in the local atomic structure around the excited atom. This dependence is significantly more pronounced than the dependence on the formal number of  $5d$  electrons. Core-to-valence RXES probes the electronic structure; consequently, we conclude that the electronic structure is similar for hexavalent oxides of Re and W, as well as for tetravalent oxides of Re and W, that crystallize in similar crystal structures.

## B. Spin-orbit interaction

The differences between  $L_2$  and  $L_3$  edges can be explained by considering dipole selection rules with SOI. We observe differences between the experimental RXES maps at the  $L_2$  and  $L_3$  edges for  $\text{ReO}_3$  and  $\text{WO}_3$ . The differences are more pronounced for  $\text{WO}_2$  and  $\text{ReO}_2$ . We discuss the results for each oxide separately.

### 1. $\text{WO}_3$

For  $\text{WO}_3$ , The high-energy part of the large diagonal streak for energy transfer of  $\sim 12$  eV is less intense at the  $L_2$  than at the  $L_3$  edge. This is reproduced in the calculated maps. There are no other significant changes.

### 2. $\text{ReO}_3$

A difference in  $\text{ReO}_3$  similar to that in  $\text{WO}_3$  is observed. Moreover, the low-energy transfer peak (with maximum at 2 eV energy transfer) becomes more intense at the  $L_2$  edge. Calculations reproduce these changes.

### 3. $\text{WO}_2$

For  $\text{WO}_2$ , the experimental RXES map at the  $L_3$  edge exhibits three peaks at energy transfer of 2, 6, and 10 eV. The peak at 6 eV has the largest intensity at the experimental  $L_3$  edge. The intensity of the low-energy transfer peak (at 2 eV energy transfer) increases considerably at the  $L_2$  edge. This peak is the most intense spectral feature at the  $L_2$  edge. A sharp peak at 6 eV energy transfer is well separated from the other features. The intensity of the peak at 10 eV decreases at the  $L_2$  edge compared to its intensity at the  $L_3$  edge. All three peaks are reproduced in the calculations for both  $L_2$  and  $L_3$  edges. Their energy positions are in excellent agreement with experiment. However, the relative intensities at the  $L_3$  edge differ from the experimental data. While the experiment shows the feature at 6 eV energy transfer as the most intense, theory overestimates the intensity of the 2 eV peak. The relative intensities between the 6 and the 10 eV features are correctly calculated. The intensity of the low-energy transfer peak at 2 eV increases significantly at the  $L_2$  edge. This is nicely reproduced in the calculations.

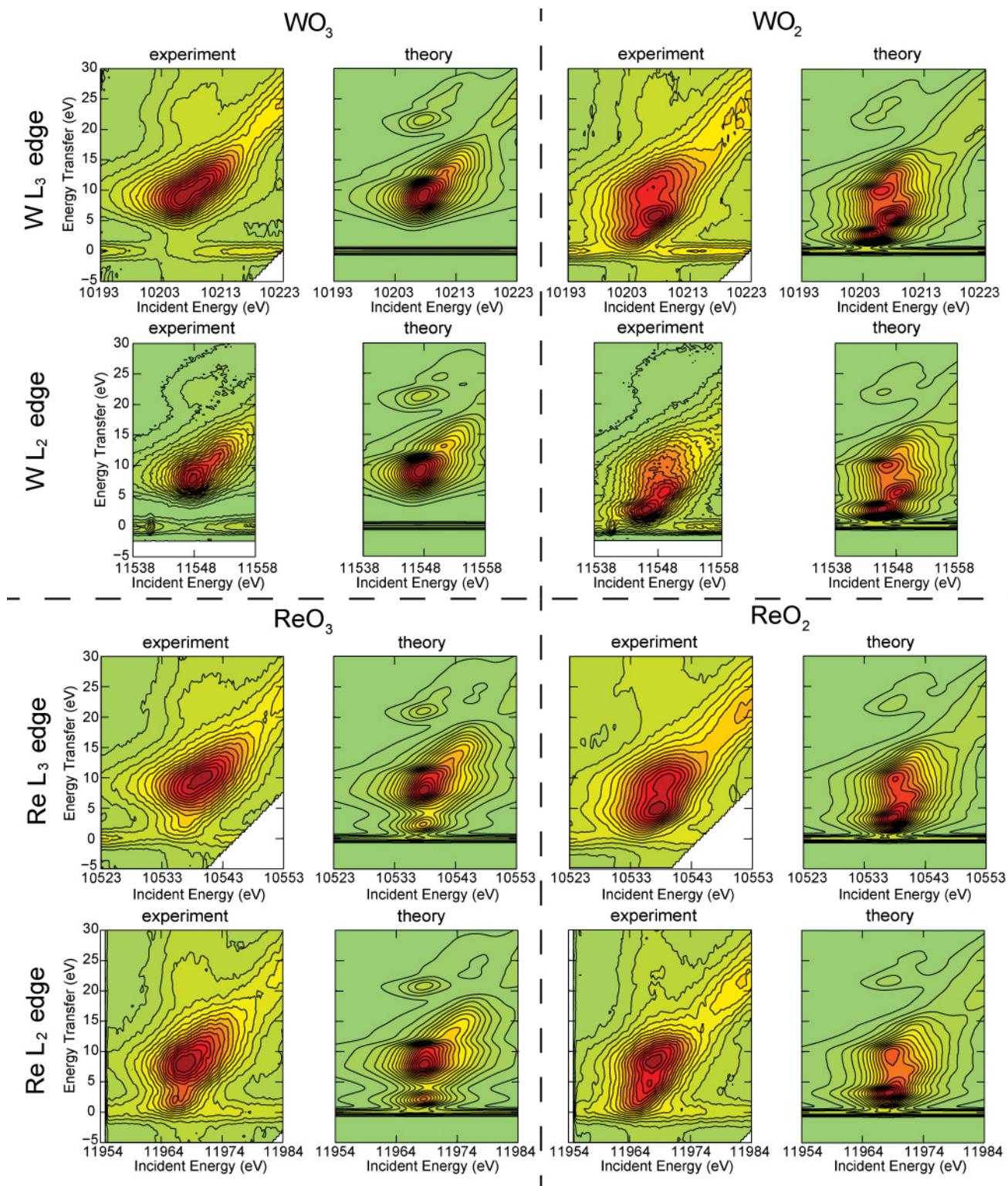


FIG. 3. (Color online) Experimental and calculated RXES planes for Re and W oxides displayed as contour maps with axes corresponding to incident and transferred energies over the Re and W  $L_2$  and the  $L_3$  absorption edges. Variations of color in the plot relate to the different scattering intensities (see Fig. 2).

4.  $ReO_2$

The experimental RXES map for  $ReO_2$  around the  $L_3$  edge has two peaks at 4 and 10 eV energy transfer, with the low-energy feature being less intense. The shoulder at

2 eV is not pronounced, unlike in  $WO_2$ . The spectral intensity is redistributed at the  $L_2$  edge RXES map, and the peak at 10 eV becomes strongest. The calculated RXES map for the  $L_3$  edge reproduces both peaks at the same energy transfer as

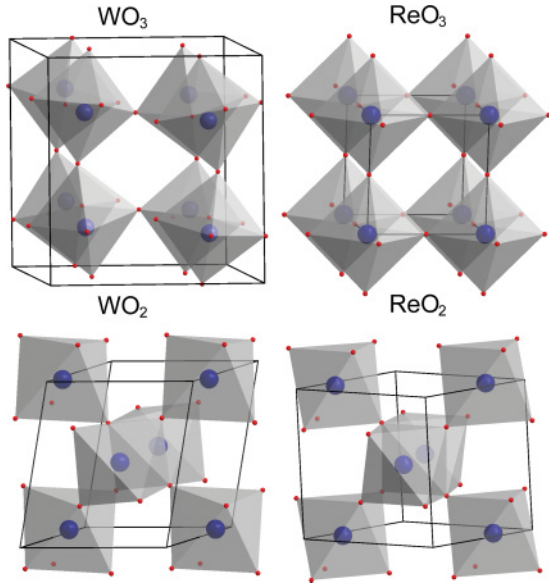


FIG. 4. (Color online) Crystal structures of the studied Re and W oxides. The thin black line shows the border of the unit cell, large blue circles are Re or W atoms, and small red dots are oxygen atoms. Octahedrons connecting oxygen atoms surrounding one metal atom are shown in gray.

in the experiment. The theoretical map for the  $L_2$  edge shows a better resolved peak at 10 eV energy transfer. The significant redistribution of intensity between the peaks at 4 and those at 10 eV energy transfer is not reproduced in the calculations.

### C. Core hole influence on RXES

The influence of the core hole has been shown to be small in many cases at the  $L_{2,3}$  edges of  $4d$  and  $5d$  transition metal compounds. The core hole screening corrections have been estimated to be  $\sim 2\%$  at the  $W L_{2,3}$  edges.<sup>27</sup> This was explained with the delocalized character of the  $d$ -orbitals.<sup>27,28</sup> Also, Ru  $L_{2,3}$  XANES spectra were successfully analyzed recently using DFT calculations without core hole but taking SOI into account in the final state.<sup>29</sup> We performed RXES calculations for the Re  $L_3$  edge in  $ReO_3$  with a supercell containing one excited atom. The supercell size was  $3 \times 3 \times 4$  unit cells, which corresponds to distances of 11 Å along the  $a$ - and  $b$ -axes and 15 Å along the  $c$ -axis between the nearest excited atoms. The final states in RXES do not exhibit a core hole, and according to the final state rule, we should use the DOS calculated without core hole for the x-ray emission process [ $\rho$  in Eq. (9)] and the excited DOS for the absorption [ $\rho'$  in Eq. (9)]. Figure 5 shows RXES maps calculated using excited (supercell) and ground state (no hole) unoccupied DOS. We observe pronounced differences in the strongest spectral features, but it is difficult to confirm the differences experimentally due to lifetime and experimental line broadening. A supercell approach corresponds to a static screening of a core hole and does not take into account many-body excitations (hole-photoelectron interaction, charge transfer excitations, *etc.*).

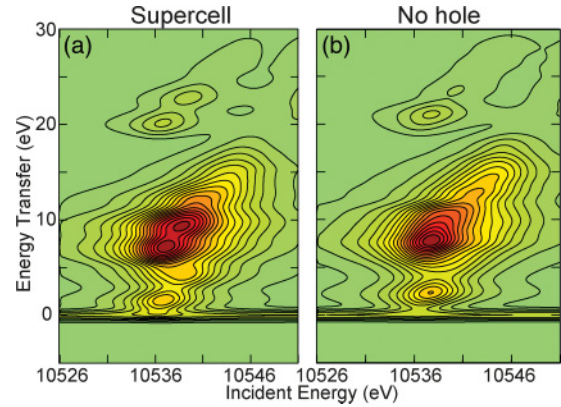


FIG. 5. (Color online) Re  $L_3$  edge RXES maps in  $ReO_3$  calculated (a) with core hole and (b) without core hole.

### D. Radial transition probability influence on RXES

Good agreement was obtained for  $ReO_3$  and  $WO_3$  for both  $L_2$  and  $L_3$  edges, while some deviations in relative peak intensities were observed for  $ReO_2$  and  $WO_2$ . The agreement between experiment and theory has to be seen in context with the experimental energy bandwidth. Possible small line splitting due to, *e.g.*, multiplet effects cannot be resolved. The calculated spectral intensities can be partly corrected by considering an energy-dependent radial transition probability—*i.e.* including a factor  $M(\epsilon) \times M(\epsilon + \omega_1 - \omega_2)$  in Eq. (9). The inset of Figure 7 shows as an example the energy-dependent radial transition probability for  $ReO_3$  that is a monotonic, smooth function. The energy dependence of the radial transition probability is similar for all studied systems. Figure 6 shows a comparison of the calculated spectra for the Re  $L_3$  edge in  $ReO_3$ . Introducing the energy-dependent radial transition probability can slightly improve the relative intensities of the peaks. This has also been observed in conventional XANES spectroscopy.<sup>8,30</sup>

### E. Discussion

Figure 7 shows the calculated partial DOS for all studied oxides. In all systems, we observe the mixing of oxygen  $s$ - and W (Re)  $d$ -states around 17 eV below the Fermi level. The energy of the oxygen  $2s$  orbital lies close to this value. Thus, the feature at energy transfer of  $\sim 20$  eV is assigned to oxygen  $2s$  states that are mixed with metal  $d$ -states.<sup>25,31</sup> This mixing allows us to determine the type of ligand, which is relevant for composite materials, as demonstrated for  $3d$  transition metals.<sup>31</sup> However, the analogy is limited because RXES at the L-edge probes the metal  $d$ -DOS, whereas the valence-to-core transition is sensitive to the metal  $p$ -DOS that is strongly mixed with the ligand orbitals.

Valence and conduction bands are formed by W or Re  $d$ -orbitals and O  $p$ -orbitals. The electron density corresponding to  $d$ -orbitals of the metal atom overlaps significantly with the electron density centered on the oxygen atom in real space. This means strong mixing between O  $p$ - and Re or W  $d$ -orbitals. Differences between  $d_{3/2}$  and  $d_{5/2}$  DOSs are visible. These differences are most pronounced in the unoccupied band and result in different intensities of the RXES features. The center of mass of the  $d_{5/2}$  band compared with that of the

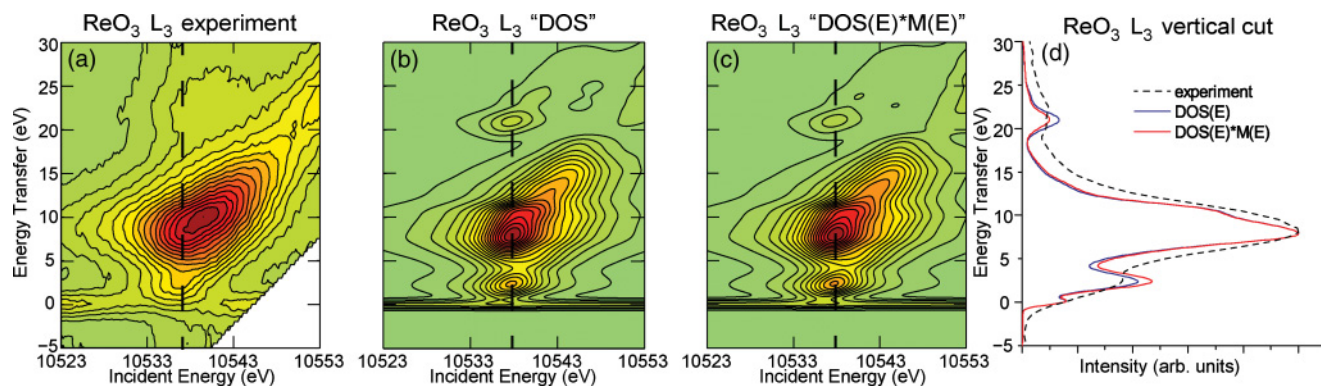


FIG. 6. (Color online) RXES maps for the Re  $L_3$  edge in  $\text{ReO}_3$ . (a) Experimental data; (b) theory using  $d$ -DOS; (c) theory using  $d$ -DOS, including energy-dependent radial transition probability  $M(E)$ ; and (d) vertical cut through RXES maps (shown as bold dashed lines in RXES maps). See the inset in Fig. 7 for  $M(E)$ .

$d_{3/2}$  band is shifted by  $\sim 0.9$ – $1.1$  eV for all studied oxides (in the integration range from  $-10$  to  $15$  eV). The value of the spin-orbit splitting parameter  $\xi_{5d}$  for these elements was estimated to be  $0.4$  eV using a nonrelativistic augmented plane wave approach.<sup>32,33</sup> Very small differences between  $5d_{5/2}$  and  $5d_{3/2}$  DOSs close to the Fermi level were obtained using the Naval Research Laboratory tight-binding model,<sup>34</sup> and this is in agreement with our results (*cf.* Fig. 7). The effect of the spin-orbit splitting becomes larger when moving away from the Fermi level. The importance of the  $5d$  SOI for the ionization spectrum of  $\text{W}(\text{CO})_6$  was proposed in Ref. 35. X-ray magnetic circular dichroism (XMCD) measurements confirmed the presence of a large SOI.<sup>36,37</sup> For example, in  $\text{Sr}_2\text{IrO}_4$ , the SOI splits the Ir  $t_{2g}$  orbitals into two levels with  $J_{\text{eff}} = 1/2$  and  $J_{\text{eff}} = 3/2$ ,<sup>4</sup> which was confirmed experimentally.<sup>2</sup> Band structure calculations showed similar results for this system.<sup>5,6</sup> Polarization-dependent RXES was measured for a single crystal of  $\text{Sr}_2\text{IrO}_4$ <sup>38</sup> with a qualitative analysis within ligand field theory. Strong SOI compared to band structure effects was reported based on an analysis of XMCD data and the branching ratio between Ir  $L_2$  and Ir  $L_3$  edges for  $\text{BaIrO}_3$ .<sup>36</sup> Within the present study, the branching ratio was not analyzed. However, we observed that band structure effects are dominant for  $5d$  systems at the beginning of the  $5d$  transition metal row. For systems with larger  $5d$  filling corrections, corresponding to intra-atomic interactions may be necessary. An investigation of the influence of different corrections to the local density approximation (SOI and Coulomb interaction parameter  $U$ ) was performed in Ref. 4 for a Ir  $5d^5$  system. Because of the extended character of  $5d$  orbitals' electron-phonon coupling is expected.<sup>39</sup> However, electron-phonon interactions are observed at energy transfer below  $1$  eV<sup>40</sup> using indirect RIXS, where the photoexcited electron participates in the emission process (see, *e.g.*, Refs. 23, 24, 40, and 41). The omission of multielectronic excitations in the present study is justified *a posteriori* by good agreement of the single-electron transition theory with the experimental data.

The following atomic charges on W and Re atoms were obtained using a charge analysis following Bader<sup>42</sup>:  $+3.0$  ( $\text{WO}_3$ ),  $+2.9$  ( $\text{ReO}_3$ ),  $+2.3$  ( $\text{WO}_2$ ), and  $+2.1$  ( $\text{ReO}_2$ ). These charges are approximately a factor of two smaller than the

formal charges as derived from the oxidation states ( $+6$  for  $\text{WO}_3$  and  $\text{ReO}_3$  and  $+4$  for  $\text{WO}_2$  and  $\text{ReO}_2$ ). Similar results were obtained recently for perovskite systems using the same analysis.<sup>43</sup>

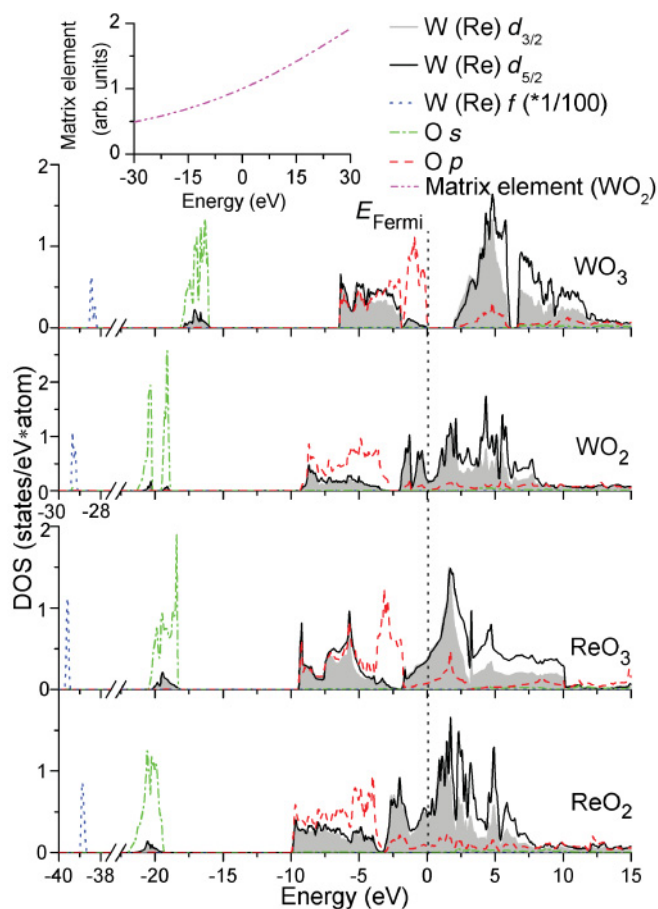


FIG. 7. (Color online) Calculated partial densities of states for Re and W oxides. Black solid lines show metal  $d_{5/2}$  states, gray-filled areas show metal  $d_{3/2}$  states, blue dotted lines show metal  $f$ -states (divided by 100), green dashed-dotted lines show oxygen  $s$ -states, and red dashed lines show oxygen  $p$ -states. The inset gives the radial transition probability (matrix element) for  $\text{ReO}_3$ .

ReO<sub>3</sub>, ReO<sub>2</sub>, and WO<sub>2</sub><sup>44,45</sup> are metals, and we do not observe a band gap. The calculated 5*d* band gap in WO<sub>3</sub> is ~1 eV smaller than what is experimentally observed. This is in line with the generally observed underestimation of the band gap in semiconductors by standard DFT.<sup>46</sup> Calculation of the total *d*-DOSs within the muffin-tin approximation using a cluster approach realized with the FEFF9 code<sup>20</sup> provides good agreement with Wien2k for WO<sub>2</sub> and ReO<sub>2</sub>.

Our theoretical approach is based on a series of approximations. The main approximations are (1) only one-electron transitions are considered, (2) the core hole is fully screened, and (3) interference effects are ignored.

(1) The calculation of the spectra using the simplified approach of Eq. (9) gives good agreement with experiment within the experimental energy bandwidth. Thus, one-electron transitions already reproduce the main spectral features. Due to the delocalized character of the 5*d* electrons, we expect correlation effects, to be less pronounced than in, *e.g.*, 3*d* transition metals. We thus neglect intra-atomic multiplet effects in the present case. This is in agreement with the analysis of XANES spectra of Pt<sup>47</sup> and Au<sup>48</sup> systems.

(2) Supercell calculations that model a core hole for ReO<sub>3</sub> show that the core hole may influence RXES. However, the comparison with experiment is not conclusive due to broad spectral features and shortcomings of the current level of theory. Our results show that a simplified approach using ground state DOS gives reasonable agreement with experimental data. Many-body effects, such as hole–photoelectron interaction and charge transfer excitations in RXES (RIXS), have to be investigated more carefully.

(3) Interference effects modify the spectral intensities. They do not modify the energies of the transitions [*cf.* Eq. (2)]. We may observe an apparent shift of a peak position in an experimental spectrum that arises from a redistribution of the spectral intensity. The satisfactory agreement between experiment and our simplified theoretical approach suggests that interference effects are weak. They may explain the rather strong discrepancies at the L<sub>2</sub> edge of ReO<sub>2</sub>.

An approach similar to ours was previously applied to Pt nanoparticles upon adsorption of CO,<sup>49</sup> and good agreement was obtained using a muffin-tin potential. The calculated unoccupied DOS and x-ray fluorescence data for occupied states with self-absorption corrections are used in the approach proposed by Hayashi *et al.*<sup>50,51</sup> based on the equation by Tulkki and Åberg.<sup>52</sup> This approach is similar to the present study and could be applied to 5*d* systems. The importance of indirect and direct RIXS processes was discussed in Ref. 41 for Cu K-edge. A real-space multiple scattering Green's function formalism was adapted for resonant inelastic x-ray scattering.<sup>53</sup> This approach is similar to ours. It has the advantage that the core hole can be easily introduced while the calculations are performed within the muffin-tin approximation. However, for L<sub>2,3</sub> edges of 4*d* systems, multielectron transitions already may be important. For the L<sub>2,3</sub> absorption edges of Ru compounds with formal 4*d*<sup>4</sup> and 4*d*<sup>3</sup> electronic configurations, multiplet effects are important, with 40% scaling of the Slater integrals with respect to the atomic values for a 4*d*<sup>4</sup> configuration and 15% scaling for a 4*d*<sup>3</sup> configuration.<sup>54</sup> For systems with more localized valence orbitals like 3*d* or 4*f*, a comprehensive treatment of multielectronic transitions

may become necessary,<sup>13</sup> and/or introduction of correction terms (local density approximation and Coulomb interaction parameter *U*, hybrid functionals, *etc.*; for a review, see Ref. 55). An Anderson impurity model construction and diagonalization of the Hamiltonian (crystal/ligand field multiplet model) is able to address multielectron excitations. This approach is well established for the analysis of systems with strong electron correlation and strong interaction of the core hole with the valence band (*e.g.*, L<sub>2,3</sub> edges in 3*d* transition metals and M<sub>4,5</sub> edges in 4*f* systems).<sup>8,13</sup> However, this model can address interatomic orbital mixing and band structure effects only through semiempirical parameters. To our knowledge, the recently developed configuration interaction approach within DFT<sup>56</sup> was not yet applied for simulation of RXES.

## VI. CONCLUSIONS

Experiments and *ab initio* single-electron band structure calculations were performed for the L<sub>2</sub> and L<sub>3</sub> RXES spectra of Re and W oxides (at the beginning of the 5*d* transition metals' row). All main spectral features were reproduced using the ground state DOS, *i.e.* neglecting the core hole potential. Significant differences between RXES spectra at L<sub>2</sub> and those at L<sub>3</sub> edges were found experimentally. These differences were reproduced by taking 5*d* SOI into account. The energy-dependent radial transition probability slightly changes the relative spectral intensities. Satisfactory agreement between experiment and theory was achieved without including core hole–induced multiplet splitting and multielectron transitions. We explain this with the delocalized character of the Re and W 5*d* electrons. This does not exclude the need for a more sophisticated theoretical approach in other systems and/or when improved spectral resolution reveals additional features. Some spectral features were assigned to x-ray emission from 4*f* states driven by quadrupole transition. Mixing of oxygen 2*s* and Re and W 5*d* orbitals was found at binding energy of ~20 eV, providing a means to identify the ligand.

The present approach allows the study of the valence band electronic structure in bulk materials with delocalized valence states and large SOI. The obtained data can be used as references for future studies of 5*d* element compounds, such as Re-based perovskite materials, Ir-based Mott insulators, and 5*d* metal–organic coordination complexes. RXES, together with a theoretical analysis based on a band structure approach, provides a powerful tool to study a large number of relevant systems with bulk sensitive hard x-rays.

## ACKNOWLEDGMENTS

We acknowledge ESRF for the provision of beam time. N.S. thanks the Russian Ministry of Education for providing the Fellowship of the President of the Russian Federation for study abroad. M.S. acknowledges financial support from the Polish Ministry of Science and Higher Education. We thank A. Kotani for useful discussions. Calculations were performed using the ESRF high-performance computers and Computer Center of the Southern Federal University.

\*Pieter.Glatzel@esrf.fr

- <sup>1</sup>D. Pesin and L. Balents, *Nat. Phys.* **6**, 376 (2010).
- <sup>2</sup>B. J. Kim, H. Ohsumi, T. Komesu, S. Sakai, T. Morita, H. Takagi, and T. Arima, *Science* **323**, 1329 (2009).
- <sup>3</sup>G. Jackeli and G. Khaliullin, *Phys. Rev. Lett.* **102**, 017205 (2009).
- <sup>4</sup>B. J. Kim, Hosub Jin, S. J. Moon, J.-Y. Kim, B.-G. Park, C. S. Leem, Jaejun Yu, T. W. Noh, C. Kim, S.-J. Oh, J.-H. Park, V. Durairaj, G. Cao, and E. Rotenberg, *Phys. Rev. Lett.* **101**, 076402 (2008).
- <sup>5</sup>S. J. Moon, H. Jin, K. W. Kim, W. S. Choi, Y. S. Lee, J. Yu, G. Cao, A. Sumi, H. Funakubo, C. Bernhard, and T. W. Noh, *Phys. Rev. Lett.* **101**, 226402 (2008).
- <sup>6</sup>A. Shitade, H. Katsura, J. Kunes, X.-L. Qi, S.-C. Zhang, and N. Nagaosa, *Phys. Rev. Lett.* **102**, 256403 (2009).
- <sup>7</sup>D. Serrate, J. M. D. Teresa, and M. R. Ibarra, *J. Phys. Condens. Matter* **19**, 023201 (2007).
- <sup>8</sup>F. M. F. de Groot and A. Kotani, *Core Level Spectroscopy of Solids* (Taylor & Francis CRC Press, Boca Raton, USA, 2008).
- <sup>9</sup>P. Glatzel and U. Bergmann, *Coord. Chem. Rev.* **249**, 65 (2005).
- <sup>10</sup>P. Glatzel, F. M. F. de Groot, O. Manoilova, D. Grandjean, B. M. Weckhuysen, U. Bergmann, and R. Barrea, *Phys. Rev. B* **72**, 014117 (2005).
- <sup>11</sup>K. Hämäläinen, D. P. Siddons, J. B. Hastings, and L. E. Berman, *Phys. Rev. Lett.* **67**, 2850 (1991).
- <sup>12</sup>J. J. Sakurai, *Advanced Quantum Mechanics* (Addison-Wesley, Los Angeles, USA, 1967).
- <sup>13</sup>A. Kotani and S. Shin, *Rev. Mod. Phys.* **73**, 203 (2001).
- <sup>14</sup>P. Blaha, K. Schwarz, G. K. H. Madsen, D. Kvasnicka, and J. Luitz, *Wien2k: An Augmented Plane Wave + Local Orbitals Program for Calculating Crystal Properties* (Karlheinz Schwarz, Techn. Universität Wien, Wien, Austria, 2001).
- <sup>15</sup>J. Jimenez-Mier, J. van Ek, D. L. Ederer, T. A. Callcott, J. J. Jia, J. Carlisle, L. Terminello, A. Asfaw, and R. C. Perera, *Phys. Rev. B* **59**, 2649 (1999).
- <sup>16</sup>J. C. Fuggle and J. E. Inglesfield, *Top. Appl. Phys.* **69** (1992).
- <sup>17</sup>ICSD database, available online at [<http://icsd.fiz-karlsruhe.de/>] (2011).
- <sup>18</sup>J. P. Perdew, K. Burke, and M. Ernzerhof, *Phys. Rev. Lett.* **77**, 3865 (1996).
- <sup>19</sup>A. H. MacDonald, W. E. Pickett, and D. D. Koelling, *J. Phys. C Solid State Phys.* **13**, 2675 (1980).
- <sup>20</sup>J. J. Rehr, J. J. Kas, M. P. Prange, A. P. Sorini, Y. Takimoto, and F. Vila, *Compt. Rendus Phys.* **10**, 548 (2009).
- <sup>21</sup>A. N. Nigam, R. B. Mathur, and R. Jain, *J. Phys. B Atom. Mol. Phys.* **7**, 2489 (1974).
- <sup>22</sup>M. A. Blokhin and I. G. Shveitser, *Handbook on X-ray Spectra* (Nauka, Moscow, 1982).
- <sup>23</sup>J. van den Brink, *Eur. Phys. Lett.* **80**, 47003 (2007).
- <sup>24</sup>L. J. P. Ament, F. Forte, and J. van den Brink, *Phys. Rev. B* **75**, 115118 (2007).
- <sup>25</sup>G. Smolentsev, A. V. Soldatov, J. Messinger, K. Merz, T. Weyhermüller, U. Bergmann, Yu. Pushkar, J. Yano, V. K. Yachandra, and P. Glatzel, *J. Am. Chem. Soc.* **131**, 13161 (2009).
- <sup>26</sup>H. Höchst and R. D. Bringans, *Appl. Surf. Sci.* **11–12**, 768 (1982).
- <sup>27</sup>A. L. Ankudinov, A. I. Nesvizhskii, and J. J. Rehr, *Phys. Rev. B* **67**, 115120 (2003).
- <sup>28</sup>A. I. Nesvizhskii and J. J. Rehr, *J. Synchrotron Radiat.* **6**, 315 (1999).
- <sup>29</sup>I. Alperovich, G. Smolentsev, D. Moonshiram, J. W. Jurss, J. J. Concepcion, T. J. Meyer, A. Soldatov, and Y. Pushkar, *J. Am. Chem. Soc.* **133**, 15786 (2011).
- <sup>30</sup>J. J. Rehr and R. C. Albers, *Rev. Mod. Phys.* **72**, 621 (2000).
- <sup>31</sup>U. Bergmann, C. R. Horne, T. J. Collins, J. M. Workman, and S. P. Cramer, *Chem. Phys. Lett.* **302**, 119 (1999).
- <sup>32</sup>L. F. Mattheiss and R. E. Watson, *Phys. Rev. Lett.* **13**, 526 (1964).
- <sup>33</sup>L. F. Mattheiss, *Phys. Rev.* **181**, 987 (1969).
- <sup>34</sup>M. M. Lach-Hab and D. A. Papaconstantopoulos, *Philos. Mag.* **88**(18-20), 2799 (2008).
- <sup>35</sup>F. Ryoichi, H. Seigo, and N. Hiroshi, *J. Chem. Phys.* **131**, 174303 (2009).
- <sup>36</sup>M. A. Laguna-Marco, D. Haskel, N. Souza-Neto, J. C. Lang, V. V. Krishnamurthy, S. Chikara, G. Cao, and M. van Veenendaal, *Phys. Rev. Lett.* **105**, 216407 (2010).
- <sup>37</sup>F. Wilhelm, P. Pouloupoulos, H. Wende, A. Scherz, K. Baberschke, M. Angelakeris, N. K. Flevaris, and A. Rogalev, *Phys. Rev. Lett.* **87**, 207202 (2001).
- <sup>38</sup>K. Ishii, I. Jarrige, M. Yoshida, K. Ikeuchi, J. Mizuki, K. Ohashi, T. Takayama, J. Matsuno, and H. Takagi, *Phys. Rev. B* **83**, 115121 (2011).
- <sup>39</sup>S. J. Moon, H. Jin, W. S. Choi, J. S. Lee, S. S. A. Seo, J. Yu, G. Cao, T. W. Noh, and Y. S. Lee, *Phys. Rev. B* **80**, 195110 (2009).
- <sup>40</sup>L. J. P. Ament, M. van Veenendaal, T. P. Devereaux, J. P. Hill, and J. van den Brink, *Rev. Mod. Phys.* **83**, 705 (2011).
- <sup>41</sup>G. Chabot-Couture, J. N. Hancock, P. K. Mang, D. M. Casa, T. Gog, and M. Greven, *Phys. Rev. B* **82**, 035113 (2010).
- <sup>42</sup>R. F. W. Bader, *J. Phys. Chem. A* **111**, 7966 (2007).
- <sup>43</sup>N. Bork, N. Bonanos, J. Rossmeisl, and T. Vegge, *J. Appl. Phys.* **109**, 033702 (2011).
- <sup>44</sup>D. B. Rogers, R. D. Shannon, A. W. Sleight, and J. L. Gillson, *Inorg. Chem.* **8**, 841 (1969).
- <sup>45</sup>F. C. Zumsteg and T. Pearsall, *Solid State Comm.* **16**, 751 (1975).
- <sup>46</sup>S. Lany and A. Zunger, *Phys. Rev. B* **78**, 235104 (2008).
- <sup>47</sup>F. M. F. de Groot, M. H. Krisch, and J. Vogel, *Phys. Rev. B* **66**, 195112 (2002).
- <sup>48</sup>J. A. van Bokhoven, C. Louis, J. T. Miller, M. Tromp, O. V. Safonova, and P. Glatzel, *Angew. Chem. Int. Ed.* **45**, 4651 (2006).
- <sup>49</sup>P. Glatzel, J. Singh, K. O. Kvashnina, and J. A. van Bokhoven, *J. Am. Chem. Soc.* **132**, 2555 (2010).
- <sup>50</sup>H. Hayashi, R. Takeda, M. Kawata, Y. Udagawa, N. Kawamura, Y. Watanabe, and S. Nanao, *Phys. Rev. B* **70**, 155113 (2004).
- <sup>51</sup>H. Hayashi, *X-ray Spectrom.* **40**, 24 (2011).
- <sup>52</sup>J. Tulkki and T. Åberg, *J. Phys. B Atom. Mol. Phys.* **13**, 3341 (1980).
- <sup>53</sup>J. J. Kas, J. J. Rehr, J. A. Soininen, and P. Glatzel, *Phys. Rev. B* **83**, 235114 (2011).
- <sup>54</sup>Z. Hu, H. von Lips, M. S. Golden, J. Fink, G. Kaindl, F. M. F. de Groot, S. Ebbinghaus, and A. Reller, *Phys. Rev. B* **61**, 5262 (2000).
- <sup>55</sup>A. Filippetti and V. Fiorentini, *Eur. Phys. J. B* **71**, 139 (2009).
- <sup>56</sup>H. Ikeno, T. Mizoguchi, and I. Tanaka, *Phys. Rev. B* **83**, 155107 (2011).